RED-PSM: Regularization by Denoising of Partially Separable Models for Dynamic Imaging

Supplementary Material

Berk Iskender[1] Marc L. Klasky[2] Yoram Bresler[1]
berki2@illinois.edu mklasky@lanl.gov ybresler@illinois.edu
[1]University of Illinois at Urbana-Champaign, USA [2]Los Alamos National Laboratory, USA

A. PSNR vs. t Comparisons

PSNR (in dB) as a function of t of frames reconstructed by the various methods for $P = 256$ for both objects is shown in Figure 8. For TD-DIP, the region between the best and the worst PSNR values for each frame for three different runs is displayed shaded to highlight the varying performance. For the warped walnut, compared to the best TD-DIP performance, RED-PSM has consistently better PSNR for all t. It also outperforms the best TD-DIP reconstructed frames in the significant majority of t for the compressed object. As expected, PSM-TV is suboptimal to other compared methods. These figures also show, for both objects, the transient behavior for all methods at the beginning and end of motion.

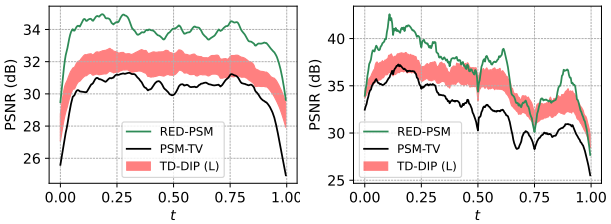

(a) Walnut (b) Compressed Material

Figure 8: Reconstruction PSNR vs time for the (a) time-varying walnut, and (b) compressed material object (Right) using different methods for $P = 256$. To highlight the varying performances of three runs with TD-DIP, the area between the best and the worst PSNR for each t is filled with red.

B. Patch-based RED denoiser

To improve the scalability of the method to higher resolution and/or 3D dynamic objects conveniently, the objective in (5) can be manipulated to operate on the patches of image frames of the time-varying object, to circumvent the need to store the complete object f in memory. This requires the denoiser D_ϕ too to operate on these patches. To showcase the potential of the suggested scheme, we replace the full-size image denoiser with a patch-based counterpart in the RED step, and compare the performance with the originally proposed method for 2D dynamic objects.

We consider $Q \times Q$-pixel partially overlapping patches with stride (i.e., relative offset in both the horizontal and vertical directions) $S < Q$, and denote by V the total number of such patches in a $J \times J$ image frame. Define the patch extraction operator $B_v : \mathbb{R}^{J^2} \to \mathbb{R}^{Q^2}$, $v \in \{0, \dots, V-1\}$ that extracts the v-th vectorized patch of the vectorized image. Then, the patch-based denoiser for RED is trained using

$$\min_{\phi} \sum_i \sum_v \|B_v f_i - D_\phi(B_v \tilde{f}_i)\|_F^2$$

where $\tilde{f}_i = f_i + \eta_i$, $\forall i$, and η_i, σ_i are set as in (8). The same data is used to train the patch-based denoiser as the full frame denoiser in (8), with data augmentation by uniformly random rotations (multiples of $\pi/2$), and random horizontal/vertical flips of each extracted patch.

The patch-based denoisers too use a DnCNN architecture and have the same configuration and training policy as the full image denoiser. In all experiments with a patch-based denoiser, a fixed patch size of 8×8 and a stride of 2 are used.

Table 3 shows that both denoiser types perform similarly using the same denoiser training policy as described in Section 5.3 for both objects, confirming the effectiveness of the patch-based RED-PSM, and its potential for highly scalable implementation. Parameter configurations for the experiments in Table 3 are provided in Table 4 in Supplementary Material C.

C. Experimental configurations

Table 5 provides PSM-TV and RED-PSM parameter selections for the experiments listed in Table 1. Likewise, Table 4 shows the parameter configurations for the denoiser type comparison experiments for RED in Table 3. Finally, Table 6 contains the architectural information for the

P	Denoiser	PSNR(dB)	SSIM	MAE	HFEN
256	Full-image	33.8	0.987	0.0004	0.315
256	Patch-based	33.7	0.989	0.0004	0.348
		(a) Walnut			
256	Full-image	35.9	0.986	0.0025	4.426
256	Patch-based	35.6	0.981	0.0027	4.559
		(b) Compressed object			

Table 3: Performance comparison for different denoiser types for RED-PSM.

DnCNN denoisers used for the two different object types throughout this work.

		(a) Walnut				(b) Comp. Material			
P	Denoiser	K	d	λ	β	K	d	λ	β
256	Full-image	10	11	5e-5	1e-4	11	13	1e-4	1e-3
256	Patch-based	10	11	5e-5	1e-4	11	13	1e-4	1e-3

Table 4: Parameter configurations for the denoiser type study experiments in Table 3.

		(a) Walnut				(b) Comp. Material			
P	Method	K	d	λ	β	K	d	λ	β
32	PSM-TV (R)	3	4	5e-2	-	3	4	10	-
32	PSM-RED-ADMM (P)	3	7	1e-4	1e-4	3	9	5.12e-2	1.6e-2
64	PSM-TV (R)	3	4	5e-2	-	5	6	10	-
64	PSM-RED-ADMM (P)	4	7	1e-4	5e-4	5	9	32e-4	4e-3
128	PSM-TV (R)	5	7	5e-2	-	8	9	5	-
128	PSM-RED-ADMM (P)	6	9	2e-4	2e-4	8	11	4e-4	2e-3
256	PSM-TV (P)	10	11	5e-2	-	11	13	10	-
256	PSM-RED-ADMM (P)	10	11	5e-5	1e-4	11	13	1e-4	1e-3

Table 5: Parameter configurations for the experiments reported in Table 1. Parameter ξ is set to $\xi = 10^{-1}$ for the walnut, and $\xi = 10^{-3}$ for the compressed object experiments.

Dataset	# of layers	# of channels	Denoising
Walnut	6	64	Direct
Comp. material	3	32	Residual

Table 6: Denoiser DnCNN configurations for the synthetically warped walnut and compressed object datasets.